Received: 4 October 2019 | Revised: 19 February 2020 | Accepted: 24 February 2020

DOI: 10.1002/sia.6764

ECASIA SPECIAL ISSUE PAPER

WILEY SURFACE and INTERFACE ANALYSIS

Orientation-dependent nanostructuring of titanium surfaces by low-energy ion beam erosion

Jens Bauer | Frank Frost

Leibniz Institute of Surface Engineering (IOM), Leipzig, Germany

Correspondence
Jens Bauer, Leibniz Institute of Surface Engineering (IOM), Permoserstrasse 15, D-04318 Leipzig, Germany.
Email: jens.bauer@iom-leipzig.de

Regular nanoscopic ripple and dot patterns are fabricated on poly-crystalline titanium samples by irradiation with 1.5 keV argon ions at normal incidence. The morphology of the nanostructures is investigated by scanning electron microscopy and scanning force microscopy. The ripple structures exhibit a saw-tooth cross-section profile. Electron backscatter diffraction experiments are performed to analyze the local grain structure. The study suggests a distinct correlation of the nanostructure morphology to the crystallographic orientation of the titanium surface.

KEYWORDS
low-energy ion beams, metals, nanostructures, titanium

1 | INTRODUCTION

Titanium has emerged a highly relevant material for biological and medical applications because it has attractive physical properties such as low-weight, resistance against corrosion, and a considerable strength combined with the high bio-compatibility of titanium oxide, which can easily be obtained via surface oxidation of a titanium device.[1] A powerful method for customization of the surface properties is nano-patterning allowing to achieve a substantially increased effective surface size, a specific local shape, or a defined surface periodicity. Hence, the combination of a tailored, inorganic surface based on titanium together with functionalized molecules or specific bio-species bears a great potential for innovative, future applications.[2]

A flexible processing tool to fabricate different kinds of nanostructured surfaces is ion beam erosion with low-energetic ions ($\leq$ 1.5 keV).[3] The technique allows the defined formation of ordered fields of nanodot or nanoripple structures by direct surface topography modification. The nanostructure formation is kinetically driven considering the interaction of the impinging ions with the surface topography and surface relaxation.[4-7] The first aspect covers the preferential sputtering in valley regions rather than on hillocks,[8,9] gradient dependent sputtering,[10] and particle-scattering effects.[11] The surface relaxation is usually discussed to result from contributions by viscous flow, ballistic drift, and thermally driven diffusion.[6] Because the contributing factors are of pure physical nature, this process is applicable to a broad variety of materials with an amorphous[12] or crystalline[13] matrix. For amorphous materials as well as crystalline materials, forming an amorphous surface layer under ion irradiation, curvature driven surface relaxation is predominant,[10] which is of minor importance on metal surfaces as result of a much enhanced intrinsic surface mobility. The nanostructure morphology can be controlled by the process parameters (ion energy, fluence, etc) and the process geometry (ion incidence angle). The ion erosion process can be further customized by an in situ chemical surface modification.[14-16] For this purpose, a reactive surface species is additionally provided during the erosion process, eg, by co-deposition. This surfactant-assisted ion erosion process can promote the surface structuring. Depending on the surfactant species, local masking effects can alter the topography formation in ion beam erosion also. In advance to the particular process conditions and surfactant effects, the substrate orientation for crystalline materials can influence the nanostructure formation. For example, in ion beam erosion on misoriented semiconductor materials as GaAs at elevated substrate temperature the formation of nanoripple structures is possible at normal ion incidence.[17] The ripple morphology can be varied by changing the misorientation angle. The driving force for orientation-dependent ripple formation is attributed to the increased adatom diffusion along dense packed crystal planes.[18] Because the diffusion on low-melting metal surfaces is enhanced, structure formation is observed already at room temperature or even below.[19]

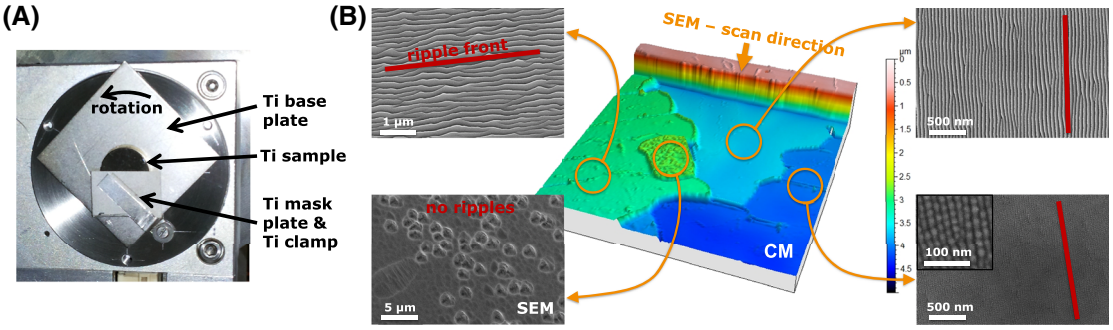

FIGURE 1 A, Rotable sample holder with titanium revetment to avoid contaminants from surrounding areas during ion beam processing. B, confocal microscope (CM) image of sample #1 measured at the erosion center position and scanning electron microscope (SEM) images representing the formed nanostructures on the grains

TABLE 1 Process conditions and obtained removal depths of the samples

	Process design		Parameters in the scan field center	
Sample	Titanium revetment	Sample rotation	Argon ion fluence	Removal depth
#1	No	No	1.1×10^{19} cm^{-2}	2.6 μm
#2	Yes	Yes	2.0×10^{19} cm^{-2}	5.0 μm
#3	Yes	No	1.4×10^{19} cm^{-2}	3.6 μm
#4	Yes	Yes	1.2×10^{19} cm^{-2}	3.6 μm

Investigations on metal surfaces have almost been done on single crystalline substrates with a predefined orientation. This study investigates the nanostructuring of polycrystalline titanium surfaces by low-energy ion beam erosion. Because many crystalline orientations are apparent on the surface, the effect of lattice alignment on the nanostructure morphology is examined in a combinatorial approach. First, the nanostructure topography is explored. Then investigations on the grain structure at the titanium surface are presented. Based on the results, correlation trends between local crystallography and nanostructure morphology are discussed.

2 | EXPERIMENTAL

An ultra high vaccum (UHV) chamber is applied with a base pressure of 2×10^{-5} Pa. A transformer coupled plasma ion source with argon (5N) gas and a triple grid extraction grid system is used for 1.5 keV ion generation. The distinct, concave grid shape allows the aperture-less generation of a constricted narrow ion beam.[20] At the machining position, the ion beam full width at half maximum is $\approx$ 5.5 mm with a total beam current of $\approx$ 1.0 mA. The process pressure is 3×10^{-3} Pa. Hence, background gas effects are expected to be negligible.

Polycrystalline pure metal titanium samples were prepared by single-point diamond turning and subsequent polishing, which reveals a flat surface with a low roughness of $\approx$ 3 nm root mean square (rms). For ion beam treatment, the sample is mounted onto a water-cooled sample holder. Deterministic processing by scanning the ion beam over a sample area allows homogeneous nanostructuring onto a broad device surface. The experiments are performed under normal ion incidence towards the sample surface. However, a possible misalignment may influence the nanostructure morphology. As already introduced, for many materials, an inclined ion incidence angle is even necessary to allow the formation of regular nanoripple structures. To avoid misinterpretations, experiments with substrate rotation have been carried out also. By that way, an unintended, slight misalignment of the ion incidence angle is eliminated. Another experimental uncertainty can be caused by contaminations during ion beam processing. Contaminations can be introduced due to an impure ion beam itself, eg, due to low-quality process gas or erosion effects inside the ion source. Because the first factor can be excluded, the latter might contribute because carbon impurities can be formed as the ion beam grids are made of graphite. Further sources of contaminations can be a considerable background gas pressure,[21] which is not assumed to be an issue in the applied UHV environment, and redeposited material by unintended peripheral sputtering from surrounding areas. Usually, the sample is mounted directly onto the aluminium sample holder and covered half by a piece of a silicon wafer thus acting as an etch mask, which itself is hold by a steel clamp. Indeed the ion beam hits those surrounding materials and redeposition into the area of interest can occur. To avoid contaminations from surrounding areas, experiments with titanium revetment are carried out also. For that purpose, the samples are placed onto a titanium base plate and covered in half by a titanium mask plate, which is held by a titanium clamp (Figure 1A). The experimental conditions of the prepared samples are summarized in Table 1.

The sample morphology is analyzed by confocal microscopy (CM; Nanofocus μsurf), scanning electron microscopy (SEM; Zeiss Gemini Ultra 55), and atomic force microscopy (AFM; Bruker FastScan). For topography evaluation, the power spectral density (PSD) function is calculated by a self-made MATLAB script (for details see Bauer and Frost[22]). From the PSD function, the nanostructure period and the surface roughness are calculated. The nanostructure cross-section profiles are derived from AFM image processing by the SPIP software (version 6.7.5 by Image Metrology). Surface orientation mapping is performed by electron-back scatter diffraction (EBSD; Bruker e^- Flash HR). The detector resolution was 320 px $\times$ 240 px with 100 ms exposure time, which reveals a hit rate well above 90% for 6 indexed bands

and 1.7° maximum band mismatch. For orientation imaging, the Bruker ESPRIT software (version 2.2) is used. A more quantitative analysis of the grain structure is done with the MTEX toolbox (version 5.2) for MATLAB.

3 | RESULTS AND DISCUSSION

Four samples are fabricated by argon ion beam processing (Table 1). Samples #1 and #2 are placed each on one half of the same piece of titanium and samples #3 and #4 in the same way on another piece of titanium. The effect of titanium revetment and sample rotation are investigated: Sample #1 is fabricated without revetment and without rotation, while sample #2 is made with revetment and rotation. The removal depth is determined at the defined mask edge by CM (Figure 1B). For sample #2, the argon ion fluence is roughly doubled and the removal depth scales in good agreement with the fluence. Hence, there is no apparent difference in the ion etching rate. This result indicates, that the possible occurrence of contaminations due to peripheral sputtering from surrounding areas, in particular from the silicon mask covering sample #1, has no significant influence on the titanium etch behaviour. Indeed, the formation of metal silicides in surfactant-assisted ion beam processing can strongly influence the etching characteristics. Furthermore, the formation of the nanostructures can even be reliant on a specific silicide surface coverage, which forms during surfactant-assisted processing in a dynamic equilibrium.[15] In the fabrication of samples #3 and #4, the effect of sample rotation only is investigated, and no effect could be observed. Hence, the sample alignment during processing is supposed to be sufficiently accurate.

The average removal depth of sample #1 is $\approx$ 2.0 μm. However, the CM measurements show height differences up to 1.5 μm between different grains of the poly-crystalline matrix, which is evidence to suggest orientation-dependent sputtering. Moreover, SEM investigations reveal different types of nanostructures on the grains (Figure 1B):

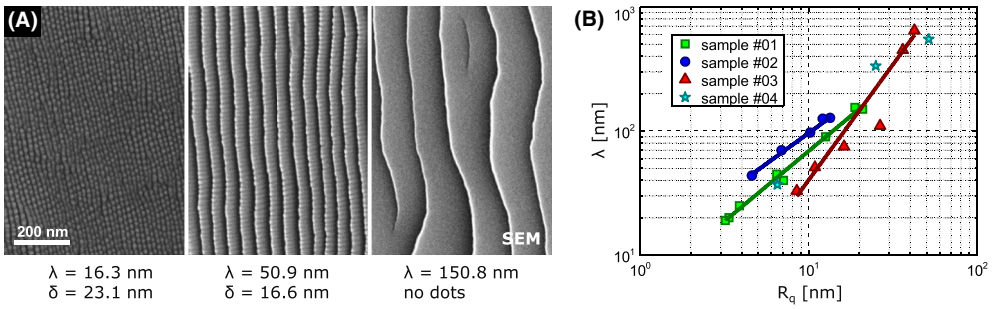

FIGURE 2 A, Scanning electron microscope (SEM) images of nanostructures with different periodicity λ (sample #1): For $\lambda < 50$ nm, nanodot patterns with dot in-line separation distance δ are formed and at higher period $\lambda > 50$ nm continuous ripple patterns are obtained. B, Nanostructure period and surface roughness follow a power-law scaling behaviour: $\lambda = m \cdot R_q^{\,n}$. The straight lines are least-square fits of the experimental data from samples #1 – #4. The obtained scaling parameters are: $m^{\{s1\}} = 5.1 \pm 0.5/n^{\{s1\}} = 1.13 \pm 0.04$, $m^{\{s2\}} = 10.0 \pm 1.0/n^{\{s2\}} = 0.99 \pm 0.05$, $m^{\{s3\}} = 0.7 \pm 0.9/n^{\{s3\}} = 1.8 \pm 0.3$. The indices s1 – s3 correspond to samples #1 – #3, respectively

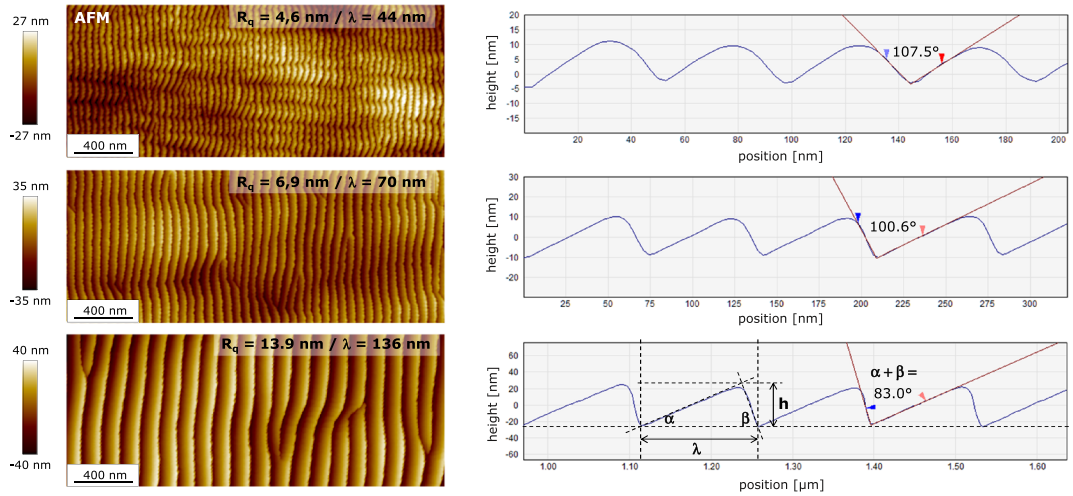

FIGURE 3 Atomic force microscope (AFM) images of ripple structures with different periods and corresponding cross-section profiles (sample #2)

ripple structures with different periodicity, ordered nanodot patterns, and smooth areas without nanostructures are found. However, each grain exhibits the same kind of structure over its whole surface area, ie, the surface morphology varies only from grain to grain.

The different types of nanostructures can be classified with respect to the pattern period λ (Figure 2A). Below a period of 50 nm, the structures appear in dot-like morphology, while above this value continuous ripple structures are found. Moreover, the detailed topography analysis by AFM and evaluation via the PSD function revealed a distinct relationship between nanostructure period and rms surface roughness R_q following a power-law scaling behaviour (Figure 2b). The scaling parameters m and n differ with respect to the experimental conditions. The results suggest a high controllability over the nanostructure morphology for a distinct process parameter set. However, presently there are no obvious relations between the scaling parameters and the experimental conditions so far. Generally, there is a power-law scaling behavior between ripple period and erosion time, while erosion time can be expressed by the removal depth too.[6] As shown in the CM measurements, there are different removal depths with respect to the local crystal alignment. Škereň et al[23] obtained similar results on crystal orientation dependent ion etching for argon ion erosion (5 keV) of thin, polycrystalline nickel films. In particular, the study suggests a correlation of the orientation-dependent etching rate to the angular dependence of the sputtering yield. Further systematic investigations are necessary to understand the effect of experimental key parameters as ion energy, ion current density, fluence, beam divergence, and substrate temperature.

In Figure 3 the cross-section geometry of ordered nanoripple structures is shown. Note, the nanostructures on samples #2-#4, which are fabricated with titanium revetment, do not differ from those of sample #1 qualitatively. The ripples exhibit a saw-tooth cross-section. The larger the structure period, the better the geometrical specificity. Within the saw-tooth geometry, the ripple height h and the surface roughness R_q are correlated via

$$h = 2\sqrt{3} \cdot R_q \tag{1}$$

To give an impression about the structure sizes, at sample #1, the structures exhibit periods of 20–200 nm and heights of 10–70 nm. At samples #3 and #4, higher periods up to 650 nm and heights up to 150 nm are found also. Additionally the cone angle $\gamma = \alpha + \beta$ of

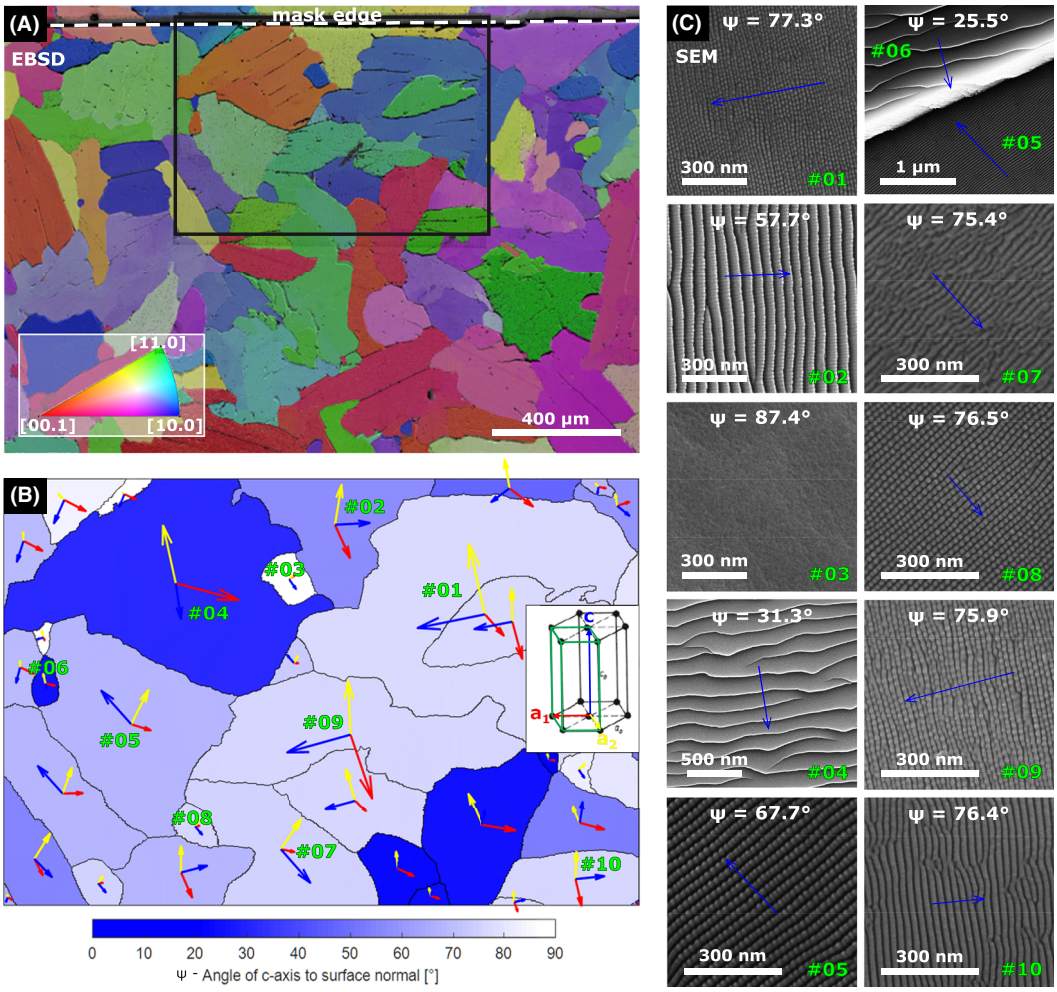

FIGURE 4 Grain orientation analysis for sample #1 by electron-back scatter diffraction (EBSD). A, Overlay image by the scanning electron microscope (SEM) image and the orientation map with inverse pole figure color coding (related to the surface normal direction). B, Grain orientation map of the boxed area in A with the surface-projected unit cell vectors a_1 (red), a_2 (yellow), and c (blue). The bluish color code corresponds to angle Ψ between the hexagonal c-axis of each grain and the surface normal direction. C, SEM images of individual grains as indexed in B. The blue arrows correspond to the surface-projected c-vector of the unit cell

the cross-section profiles can be directly determined as illustrated in Figure 3. From γ, the saw-tooth slope angles α and β can be separated via

$$\frac{\lambda}{h} = \frac{1}{\tan\alpha} + \frac{1}{\tan\beta} \quad (2)$$

As a result, the ripple topography can be fully described by the geometrical parameters: period, height, and both slope angles.

EBSD experiments are performed to analyze the local crystal structure (Figure 4A). Up to 1155 K titanium is thermodynamically stable in the hexagonal α-phase. The MTEX toolbox for MATLAB is applied for EBSD data evaluation and grain recognition. The rhombohedral unit cell is described by the lattice vectors a_1 and a_2, which lie in-plane in the dense packed (00.1) plane, and lattice vector c, which is directed parallel to [00.1] (see the structure inset in Figure 4b). Figure 4b illustrates the tilt angle Ψ between the c-axis and the surface normal for the grain structure of sample #1. A dark blue color corresponds to only a slight tilt between the crystallographic c-axis and the normal vector, while a very bright color indicates that the c-axis of the particular grain lies almost within the sample surface plane. In Figure 4C, SEM images of the grains are shown. As a general trend, the structure period increases for lower Ψ-angles. A Ψ-angle of 60° corresponds to a structure period of about 50 nm. Thus, continuous ripple structures are obtained for $\Psi < 60°$, while nanodot patterns are achieved for $\Psi > 60°$ (see also Figure 2A). For grain #03, the Ψ-angle is almost 90°, and no nanostructures are observed but a smooth surface. The arrows in Figure 4C illustrate the direction of the c-vector projected to the surface plane. The nanostructure propagation direction is oriented along the projected c-vectors. Hence, not only the nanostructure morphology but also their in-plane alignment are found to be correlated to the crystallographic orientation of the titanium grain structure.

Qian and Zhou[24] reported on the nanoripple formation at titanium surface after irradiation with midenergy gallium ions (30 keV). However, despite ripples were also observed at normal ion incidence, an incidence angle of 15° was necessary, in which a crystal orientation dependent formation was obtained. Argon ion irradiation experiments at nickel films reveal even higher incidence angles of 70° or 80° to be necessary for ripple formation.[23] However, the nickel grain sizes are very tiny, and the ripples formed at high incidence angles comprise a large amount of grains, which indicates that those formation conditions are not correlated to any crystal alignment effect but the distinct experimental process geometry at grazing ion incidence. In contrast, in the present study already at normal ion incidence, the local crystal structure determines the nanostructure formation. If surface adatom diffusion is the major driving force, crystal facets with higher diffusion coefficients will determine the forming etch morphology corresponding to the equilibrium crystal etch shape. Actually, the adatom diffusion on the hexagonal dense packed titanium (00.1) plane is predicted to be exceedingly fast.[25] In this view, the top facets of the ripples would be (00.1). Indeed, the experiments show increasing ripple terraces, if the Ψ-angle becomes lower, ie, the c-axis nears the surface normal. Also the in-plane ripple alignment dependency on the surface-projected c-axis matches this view. However, more systematic investigations are necessary to prove this hypothesis for normal ion incidence and to study the limitations due to specific process conditions.

4 | CONCLUSIONS

In summary, the formation of regular nanostructures is observed on titanium surfaces after low-energy argon ion irradiation at normal incidence. With respect to the periodicity, continuous ripple patterns or regular arrays of nanodots are obtained. The nanostructure period and the surface roughness, which is directly related to the nanostructure height, are correlated and follow a power-law scaling behaviour. The investigations suggest, that the nanostructure topography is determined by the local crystallographic alignment of the grains at the surface rather than by the process conditions of ion beam machining or by surfactant-related effects. The periodicity of the nanostructure is defined by the angle between the hexagonal c-axis of the titanium unit cell and the surface normal. The higher this angle, the lower the nanostructure period. If the c-axis is perpendicular to the surface normal, no nanostructures but a smooth surface is found. The in-plane alignment of the nanostructures is determined by the c-axis direction projected to the surface, while the projected c-axis direction is oriented parallel to the nanostructure propagation direction.

ACKNOWLEDGMENTS

The authors wish to acknowledge Dr R. Beutner (TU Dresden) for sample preparation and D. Hirsch is thanked for SEM measurements.

ORCID

Jens Bauer https://orcid.org/0000-0002-4339-8296
Frank Frost https://orcid.org/0000-0002-4043-6314

REFERENCES

1. Liu X, Chu P, Ding C. Surface modification of titanium, titanium alloys, and related materials for biomedical applications. *Mater Sci Eng R Reports*. 2004;47(3-4):49-121. https://doi.org/10.1016/j.mser.2004.11.001
2. Sommerfeld J, Richter J, Niepelt R, et al. Protein adsorption on nano-scaled, rippled TiO2 and Si surfaces. *Biointerphases*. 2012;7(1-4):1-7. https://doi.org/10.1007/s13758-012-0055-5
3. Frost F, Ziberi B, Schindler A, Rauschenbach B. Surface engineering with ion beams: from self-organized nanostructures to ultra-smooth surfaces. *Appl Phys A Mater Sci Process*. 2008;91(4):551-559. https://doi.org/10.1007/s00339-008-4516-0
4. Bradley RM, Harper JME. Theory of ripple topography induced by ion bombardment. *J Vac Sci Technol A Vacuum, Surfaces, Film*. 1988;6(4):2390-2395. https://doi.org/10.1116/1.575561
5. Makeev MA, Cuerno R, Barabási AL. Morphology of ion-sputtered surfaces. *Nucl Instruments Methods Phys Res Sect B Beam Interact Mater Atoms*. 2002;197(3-4):185-227. https://doi.org/10.1016/S0168-583X(02)01436-2
6. Frost F, Fechner R, Ziberi B, Völlner J, Flamm D, Schindler A. Large area smoothing of surfaces by ion bombardment: fundamentals and applications. *J. Phys. Condens. Matter*. 2009;21(22):224026. https://doi.org/10.1088/0953-8984/21/22/224026
7. Keller A, Facsko S. Ion-induced nanoscale ripple patterns on Si surfaces: theory and experiment. *Mater (Basel)*. 2010;3(10):4811-4841. https://doi.org/10.3390/ma3104811

8. Sigmund P. Theory of sputtering. *Phys Rev*. 1969;184(2):383-416. https://doi.org/10.1103/PhysRev.184.383
9. Sigmund P. A mechanism of surface micro-roughening by ion bombardment. *J Mater Sci*. 1973;8(11):1545-1553. https://doi.org/10.1007/BF00754888
10. Nobes MJ, Colligon JS, Carter G. The equilibrium topography of sputtered amorphous solids. *J Mater Sci*. 1969;4(8):730-733. https://doi.org/10.1007/BF00742430
11. Teichmann M, Lorbeer J, Frost F, Rauschenbach B. Ripple coarsening on ion beam-eroded surfaces. *Nanoscale Res Lett*. 2014;9(1):439. https://doi.org/10.1186/1556-276X-9-439
12. Toma A, De Mongeot FB, Buzio R, et al. Ion beam erosion of amorphous materials: evolution of surface morphology. *Nucl Instrum Method Phys Res Sect B Beam Interact Mater Atoms*. 2005;230(1-4):551-554. https://doi.org/10.1016/j.nimb.2004.12.099
13. Madi CS, Bola George H, Aziz MJ. Linear stability and instability patterns in ion-sputtered silicon. *J. Phys. Condens. Matter*. 2009;21(22). https://doi.org/10.1088/0953-8984/21/22/224010
14. Kree R, Yasseri T, Hartmann AK. Surfactant Sputtering: Theory of a new method of surface nanostructuring by ion beams. *Nucl Instrum Methods Phys Res Sec B: Beam Interact Mater Atom*. 2009;267(8-9):1403-1406. https://doi.org/10.1016/j.nimb.2009.01.150
15. Engler M, Frost F, Müller S, et al. Silicide induced ion beam patterning of Si(001). *Nanotechnology*. 2014;25(11):115303. https://doi.org/10.1088/0957-4484/25/11/115303
16. Muñoz-García J, Vázquez L, Castro M, et al. Self-organized nanopatterning of silicon surfaces by ion beam sputtering. *Mater Sci Eng R Rep*. 2014;86:1-44. https://doi.org/10.1016/j.mser.2014.09.001
17. Engler M, Škereň T, Facsko S. Nano patterns self-aligned to Ga dimer rows on GaAs surfaces. *Conden Matter*. 2016;1611:06836. arXiv:1611.06836.
18. Chan WL, Chason E. Making waves: Kinetic processes controlling surface evolution during low energy ion sputtering. *J Appl Phys*. 2007;101(12). https://doi.org/10.1063/1.2749198
19. Costantini G, Rusponi S, Buatier De Mongeot F, Boragno C, Valbusa U. Periodic structures induced by normal-incidence sputtering on Ag(110) and Ag(001): flux and temperature dependence. *J Phys Conden Matter*. 2001;13(26):5875-5891. https://doi.org/10.1088/0953-8984/13/26/303
20. Bauer J, Ulitschka M, Pietag F, Arnold T. Improved ion beam tools for ultraprecision figure correction of curved aluminum mirror surfaces correction of curved aluminum mirror surfaces. *J Astron Telesc Instrum Syst*. 2018;4(4):046003. https://doi.org/10.1117/1.JATIS.4.4.046003
21. Hofer W, Bay H, Martin P. Sputter-erosion and impurity emission from titanium and vanadium at low-energy ion bombardment. *J Nucl Mater*. 1978;76-77:156-162. https://doi.org/10.1016/0022-3115(78)90129-0
22. Bauer J, Frost F, Arnold T. Reactive ion beam figuring of optical aluminium surfaces. *J Phys D Appl Phys*. 2017;50(8):085101. https://doi.org/10.1088/1361-6463/50/8/085101
23. Škereň T, Temst K, Vandervorst W, Vantomme A. Ion-induced roughening and ripple formation on polycrystalline metallic films. *New J Phys*. 2013;15:093047. https://doi.org/10.1088/1367-2630/15/9/093047
24. Qian HX, Zhou W. Self-organization of ripples on Ti irradiated with focused ion beam. *Appl Surf Sci*. 2012;258(6):1924-1928. https://doi.org/10.1016/j.apsusc.2011.06.152
25. Liu WC, Woo CH, Huang HC. Diffusion and clustering on the titanium (0001) surface. *J Comput Mater Des*. 1999;6(2-3):311-321. https://doi.org/10.1023/A:1008783311498

How to cite this article: Bauer J, Frost F. Orientation-dependent nanostructuring of titanium surfaces by low-energy ion beam erosion. *Surf Interface Anal*. 2020;52:1071–1076. https://doi.org/10.1002/sia.6764